SANDIA REPORT

SAND97–0805 • UC–706
Unlimited Release
Printed April 1997

Hazards of Falling Debris to People, Aircraft, and Watercraft

J. Kenneth Cole, Larry W. Young, Terry Jordan-Culler

Prepared by
Sandia National Laboratories
Albuquerque, New Mexico 87185 and Livermore, California 94550

Sandia is a multiprogram laboratory operated by Sandia Corporation, a Lockheed Martin Company, for the United States Department of Energy under Contract DE-AC04-94AL85000.

Sandia National Laboratories

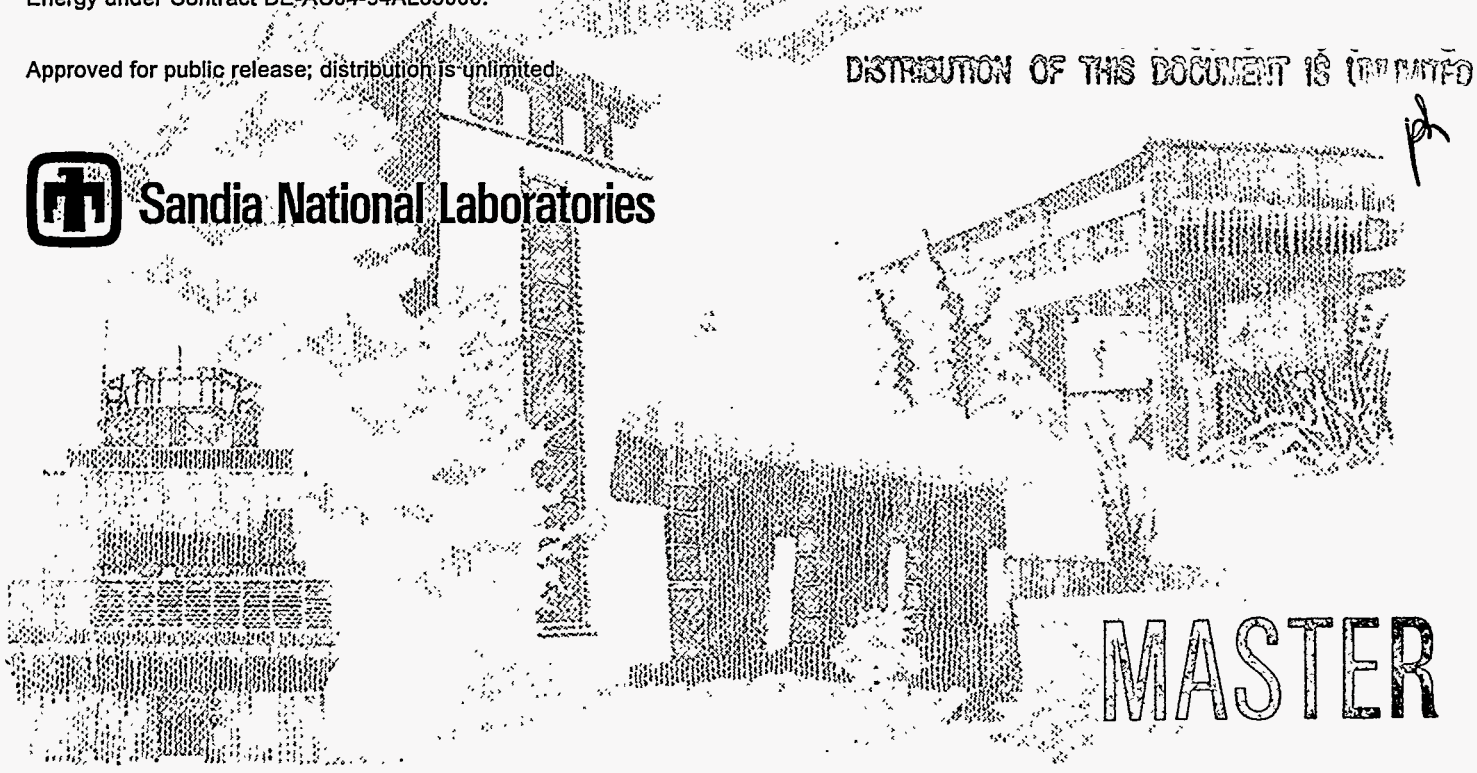

Issued by Sandia National Laboratories, operated for the United States Department of Energy by Sandia Corporation.

Available to DOE and DOE contractors from
Office of Scientific and Technical Information
P.O. Box 62
Oak Ridge, TN 37831

Prices available from (615) 576-8401, FTS 626-8401

Available to the public from
National Technical Information Service
U.S. Department of Commerce
5285 Port Royal Rd
Springfield, VA 22161

NTIS price codes
Printed copy: A03
Microfiche copy: A01

SAND97-0805
Unlimited Release
Printed April 1997

Distribution
Category UC-706

Hazards of Falling Debris to People, Aircraft, and Watercraft*

J. Kenneth Cole,
Larry W. Young and
Terry Jordan-Culler
Aerosciences and Compressible
Fluid Mechanics Department
Sandia National Laboratories
P. O. Box 5800
Albuquerque, NM 87185-0825

Abstract

This report is a collection of studies performed at Sandia National Laboratories in support of Phase One (inert debris) for the Risk And Lethality Commonality Team. This team was created by the Range Safety Group of the Range Commander's Council to evaluate the safety issues for debris generated during flight tests and to develop debris safety criteria that can be adopted by the national ranges.

Physiological data on the effects of debris impacts on people are presented. Log-normal curves are developed to relate the impact kinetic energy of fragments to the probability of fatality for people exposed in standing, sitting, or prone positions. Debris hazards to aircraft resulting from engine ingestion or penetration of a structure or windshield are discussed. The smallest mass fragments of aluminum, steel, and tungsten that may be hazardous to current aircraft are defined. Fragment penetration of the deck of a small ship or a pleasure craft is also considered. The smallest mass fragments of aluminum, steel, or tungsten that can penetrate decks are calculated.

* The work described in this report was performed for the White Sands Missile Range under U.S. Army MIPR Nos. W43STM96385AR, W43STM97127NV, and W43STM97196AR.

Acknowledgments

The authors wish to thank the following people:

Mr. Jerry Haber ACTA	for clarifying the use of log-normal functions, maximum likelihood fits of probability of fatality data, and suggestions which improved the ship hazard section.
Mr. Tom Pfitzer APT-Research, Inc.	for promoting the log-normal function to describe the probability of fatality vs. kinetic energy data.
Dr. Paul Jaramillo APT-Research, Inc.	for providing information on aircraft construction typical of small business jets.
Mr. Brad Hill Mr. Scott Price TYBRIN Corporation	for suggestions which improved the description of the log-normal functions and a quick method for applying them.

A sub-group of the Risk And Lethality Commonality Team was formed to study the available data on human impact vulnerability and to recommend how this information should be presented to be readily used by safety personnel. The members of this sub-group were:

Mike Meehan,	White Sands Missile Range,
Brad Hill,	TYBRIN Corporation,
Jerry Esquibel,	USAKA/Kwajalein Missile Range,
Tom DeLong	U. S. Army Space & Strategic Defense Command
Ken Cole,	Sandia National Laboratories.

Table of Contents

List of Figures

List of Tables

1 Introduction

The Risk And Lethality Commonality Team (RALCT) was formed in February 1996 at the direction of the Range Safety Group of the Range Commander's Council. The team consisted of representatives from the national test ranges as well as technical consultants from industry and government agencies. Weston Wolff, Chief of the Flight Safety Office, White Sands Missile Range, was the chairman for the Phase One effort which addressed inert debris. RALCT's initial purpose was to evaluate the safety issues of intentional or accidental generation of inert debris by flight tests at national test ranges. This debris can vary from hardware shed during normal missile operation to fragments generated by explosion, hypervelocity collision, aerothermal breakup, or a flight termination system. The second purpose of the RALCT was to review the safety criteria for inert debris currently being used by each range and to recommend debris safety standards that could be adopted by all of the national ranges.

This report is a collection of the studies that were performed for the RALCT by Sandia National Laboratories. Some of the topics presented here were not included in the proposed Standard or the Supplement published by the team. Section 6, Bibliography, contains many more entries, particularly for debris hazards to personnel, than are referred to in this report. They are grouped according to topic and alphabetically by author. It is hoped that providing the reader with a more complete overview of these subjects will encourage future studies to better quantify the range safety criteria used. Note that mixed units are intentionally used in this report to be compatible with those more frequently used by practicing safety personnel.

2 Debris Hazardous To People

2.1 Development Of Probability Of Fatality Curves

Debris generated by exo- and endo-atmospheric tests can be hazardous to people that are in the areas where the debris reaches the earth's surface. The amount of land and sea area that must be controlled to minimize danger to people from falling debris depends upon the levels of debris mass, momentum, and energy required to cause injury or death.

Feinstein, Heugel, Kardatzke, and Weinstock[13] reported in a 1968 Illinois Institute of Technology (IIT) Research Institute publication on the effects of blast, debris, and thermal and nuclear radiation on sheltered and unsheltered personnel. The physiological data upon which they based their analyses were obtained from experiments that had been performed for the Department of Defense on live animals, human cadavers, and skin and gelatin models. They found that the severity of cutting and penetrating injuries correlated best with the impacting fragment's energy times velocity squared, mv^4, crushing and tearing with energy, mv^2, and impulse loading with momentum, mv. Table 2.1 summarizes these different types of injuries with judgements by Feinstein et al as to their possible severity and mortality rate, i.e., the probability that an injury will result in death.

Table 2.1: Characteristics of fragment impact injuries, according to Feinstein et al.

Severity	Types of Injury	Dose Relationship	Mortality Rate
Superficial	Glass and other lacerations	mv^4	10%
	Unilateral lung hemorrhage	mv	
	Rib fractures	mv	
Incapacitating	Glass and other missile penetrations	mv^4	30%
	Bone abrasions and cracking	mv^2	
	Internal lacerations from fractured ribs	mv^2	
Near lethal	Bilateral hemorrhage	mv^4	70%
	Skull fracture	mv^2	
	Passage through abdomen or other lethal areas	mv^4	
Lethal	Passage through thorax (Fatal within 1hr)	mv^4	100%

Feinstein divided the body into three parts: the head, the thorax, and the abdomen and limbs. Then using the injury data, curves for each body part were defined for the threshold of serious injury and kill probabilities of 0.1, 0.5 and 0.9. Figures 2.1-2.3 show these curves as solid lines. Also,

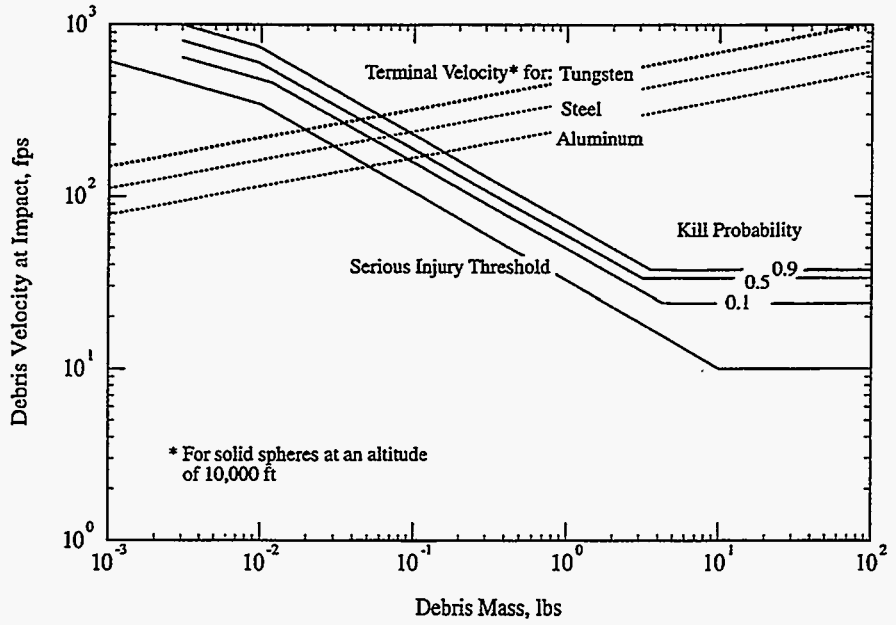

Figure 2.1: Kill probability from debris impacts to the head.

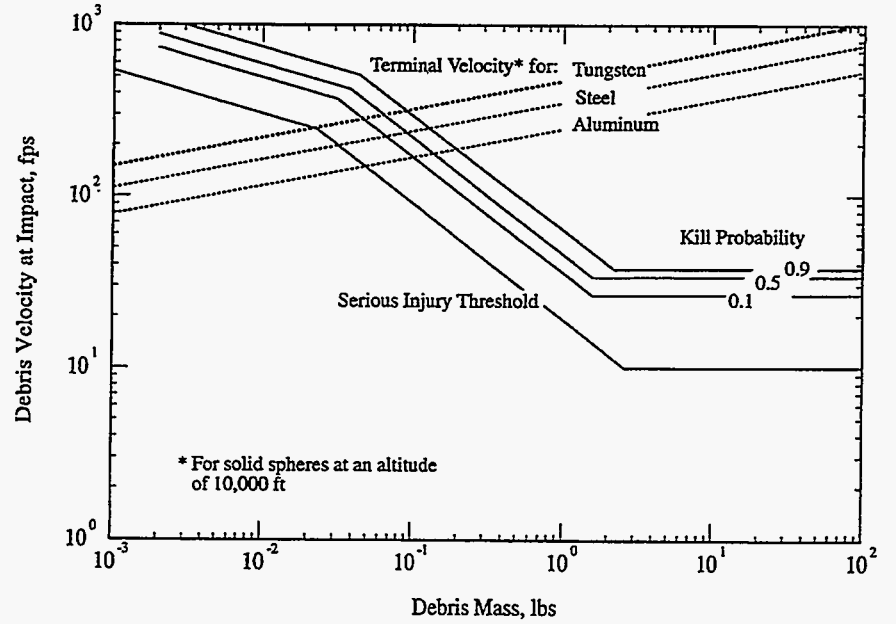

Figure 2.2: Kill probability from debris impacts to the thorax.

included in these figures are dotted-line curves for the speed that an aluminum, steel, or tungsten solid spherical fragment would possess on reaching terminal velocity at an altitude of 10,000 ft. Only fragments that have dart or cone like shapes and are aerodynamically stable can have greater terminal velocities for a given mass. It is extremely unlikely that such stable shapes would be

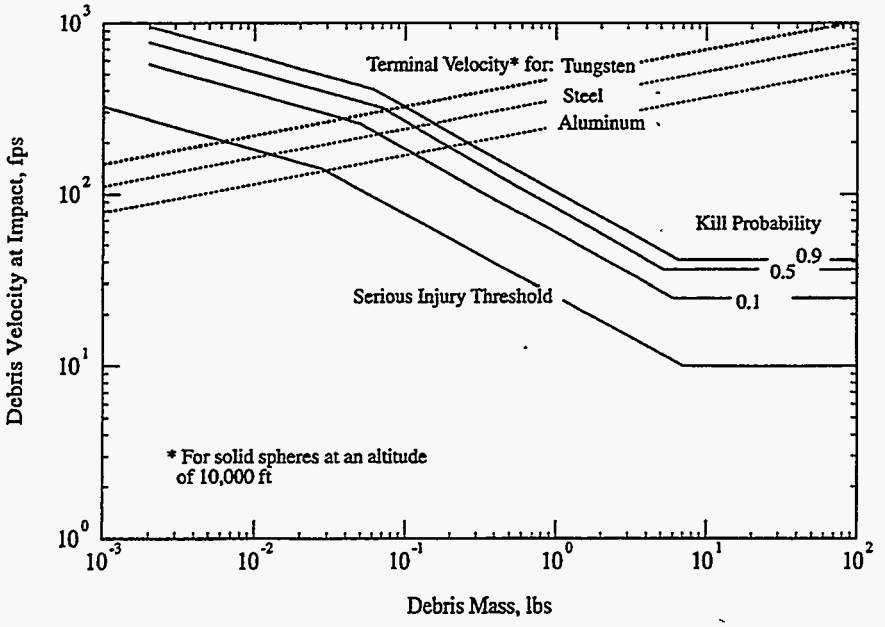

Figure 2.3: Kill probability from debris impacts to the abdomen & limbs.

created in most debris generation processes. The altitude of 10,000 ft was used to be conservative. Most human habitation occupies lower altitudes where the terminal velocities are less.

Smaller mass fragments which lie to the left of the intersection of a terminal velocity curve with a Feinstein curve represent a lower kill probability since they cannot attain the higher velocity required. This method of terminal velocity screening does not apply when the fragments have not traveled a sufficient distance through the atmosphere to decelerate to a terminal condition before impact.

The center portion of each Feinstein kill probability curve is that part between its intersection with a terminal velocity curve on the left and the abrupt shift to zero slope on the right. For the head and for the abdomen & limbs, this portion has a slope which represents nearly constant kinetic energy, mv^2. For the thorax, the center portion has a slightly greater slope and is closer to $mv^{1.5}$.

Translation casualty data was used by Feinstein to define the kill probability curves for the fragments with mass greater than 2-8 lb where the curves have zero slope, i.e., constant velocity. These data were based partially upon fatality data from urban automobile accidents where people were thrown forward by the deceleration. In the region of zero slope the fragment kinetic energy increases linearly with mass. Thus, the kinetic energies represented by the center portion of each kill probability curve are the lowest that can produce that kill probability. Using these kinetic energies for the larger fragments, therefore, give conservative results. If lethality data or analyses become available for the larger debris, they should be used in lieu of the analysis that follows.

S-curves for the probability of fatality were constructed as a function of the fragment kinetic energy. To do so required that an effective kinetic energy be determined for each Feinstein

probability of fatality curve for each body part. Figure 2.4 shows a typical Feinstein probability of fatality curve whose central portion is represented by $mv^b = k$. An effective average kinetic energy was calculated first as an unweighted average between points 1 and 2. Point 1 is the intersection of the terminal velocity curve and the Feinstein curve and point 2, the place where the slope of the Feinstein curve changes to zero. The equation for this unweighted average is:

$$\overline{KE} = \frac{1}{(m_2 - m_1)} \int_{m_1}^{m_2} (KE)\, dm \tag{2.1}$$

where: $\overline{KE}$ = average kinetic energy,
KE = fragment kinetic energy,
m_i = fragment mass at point i, $i = 1,2$.

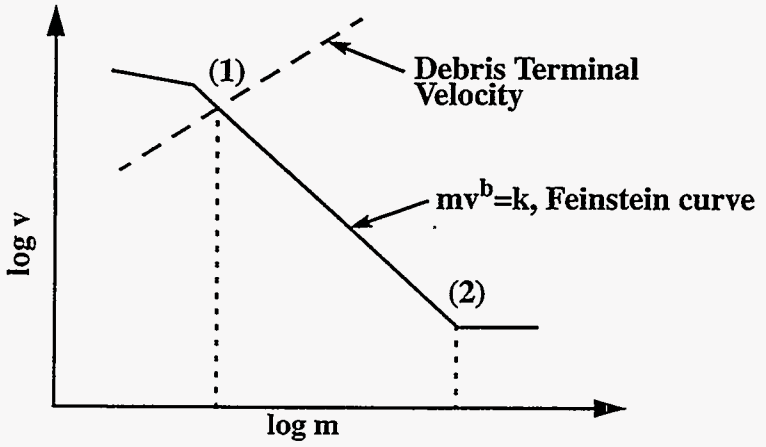

Figure 2.4: Illustration of region used to define average kinetic energy.

From hypervelocity collisions,[48, 49] it has been observed that the number of fragments increases rapidly as the mass of the fragments becomes smaller. Hence, it was decided that an average weighted toward the more numerous, lower mass, fragments should be used. This was accomplished with a log-weighted average. The log-weighted average reduces to:

$$\overline{KE}_{Weighted} = \frac{1}{(\log m_2 - \log m_1)} \int_{m_1}^{m_2} \left(\frac{KE}{m}\right) dm \tag{2.2}$$

For the head and abdomen & limbs, the weighted and unweighted averages of kinetic energy are nearly identical. However, for the thorax, the weighted average gives a slightly larger value than the unweighted average.

Feinstein et al employed log-normal distributions to relate the severity of each type of injury to the impact dose. In this analysis, the log-normal relationship was adopted to describe the probability of fatality versus the effective kinetic energy for impacts to the head, thorax, and abdomen & limbs. Figure 2.5 shows log-normal S-curves for each body part and includes a table which lists the kinetic energy at 10, 50 and 90% probability of fatality as well as the log-normal parameters.

The form of the natural log-normal equation used to calculate these curves is:

$$P_i\langle Fatality|KE < K\rangle = \int_0^K \frac{1}{x\beta_i\sqrt{2\pi}} e^{\left\{\frac{-(\ln x - \ln\alpha_i)^2}{2\beta_i^2}\right\}} dx \qquad (2.3)$$

where: K = fragment impact kinetic energy, ft-lbf,

α_i = scale parameter, the median for log-normal, ft-lbf,

β_i = shape parameter for log-normal.

This equation can be evaluated for different values of kinetic energy through numerical integration. A simpler technique is to correlate an impact kinetic energy to a probability of fatality. This process starts with the equation:

$$Z = \frac{\ln(KE) - \ln(\alpha_i)}{\beta_i} \qquad (2.4)$$

Assuming a cumulative normal distribution, Z is the number of standard deviations that *ln(KE)* is removed from $ln(\alpha_i)$. Once a Z is calculated for a given kinetic energy, the probability of fatality can be determined by using a normal distribution table. These tables are found in most statistics textbooks and mathematical and engineering handbooks.

For example, if α_i = 55 ft-lbf and β_i = 0.2802, a kinetic energy of 78.8 ft-lbf will result in a value of Z = 1.28. In a normal distribution table, this Z value corresponds to a probability of 90%. A kinetic energy of 38.4 ft-lbf will result in a value of Z = -1.28, which corresponds to a probability of 10%. A kinetic energy of 55 ft-lbf produces Z = 0.0, which corresponds to a probability of 50%.

In everyday circumstances, the body part impacted by an inert debris fragment will not be known a priori. Hence, the probabilities derived for the three body parts must be combined to handle

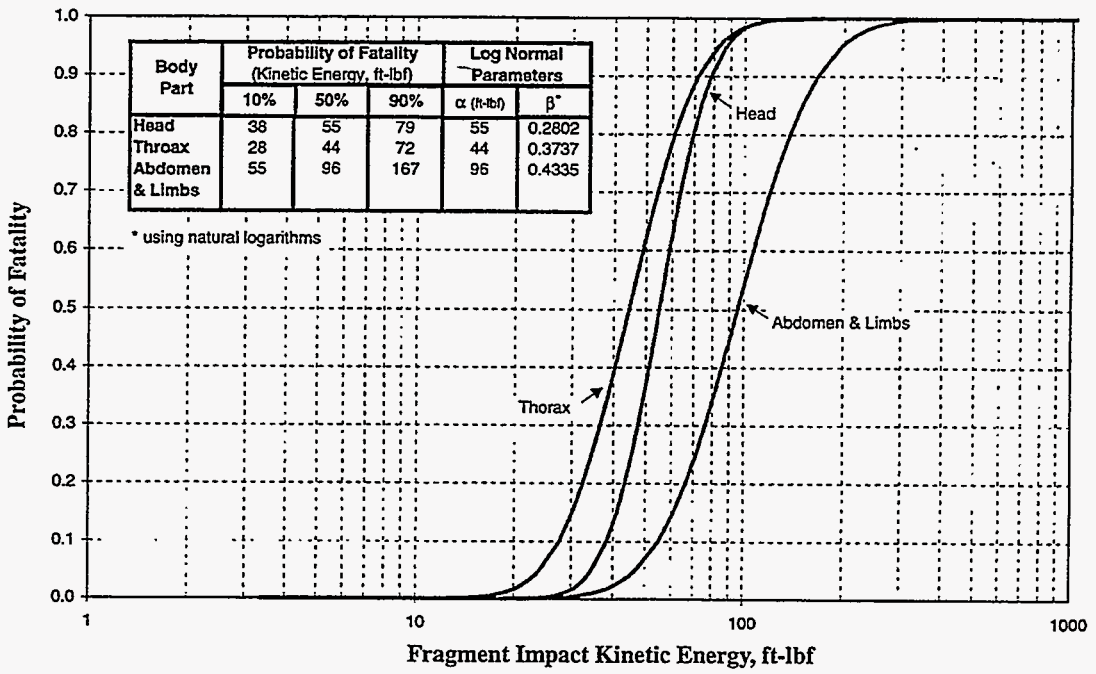

Figure 2.5: Probability of fatality from debris impacts to different body parts.

more general situations. Given that a person is hit, the conditional probability of hitting a particular body part is equal to the ratio of the area that part presents to the total area presented by the person. The more general probabilities of fatality curves were obtained by combining the probability of fatality curves for the three body parts through the use of standard-man dimensions. In doing this an implicit assumption was made that each fragment was sufficiently small that it struck only one body part. Further, it was assumed that a body part was equally vulnerable when impacted from any direction. No benefit was taken for the distribution of bony and muscular mass. Figure 2.6 shows the standard man which was obtained from Janser.[21] The body proportions of the sketch do not exactly correspond to the dimensions included with the sketch. A detailed body description with corrected proportional areas was made by Bradley Hill,[20] of TYBRIN Corporation. The weighting given to each body part was defined as the ratio of the area that body part presents to the area the total body presents for impact. This weighting changes as a function of the person's position and the angle the debris velocity vector makes to the person. Body positions selected were standing, sitting, and prone. Table 2.2 lists the area ratios for the three body parts when the debris is falling nearly vertically.

A composite curve was generated for each of the three body positions based on the equation:

$$P_j(KE) = \sum_{i=1}^{3} A_{ij} P_i(KE) \qquad (2.5)$$

where P_i = Probability of fatality for body part (i), derived from log-normal curve,
P_j = Probability of fatality for body position (j),
KE = Kinetic energy of impacting debris in ft-lbf,
A_{ij} = Weighting of body part (i) for body position (j), see columns 3-5 of Table 2.2.

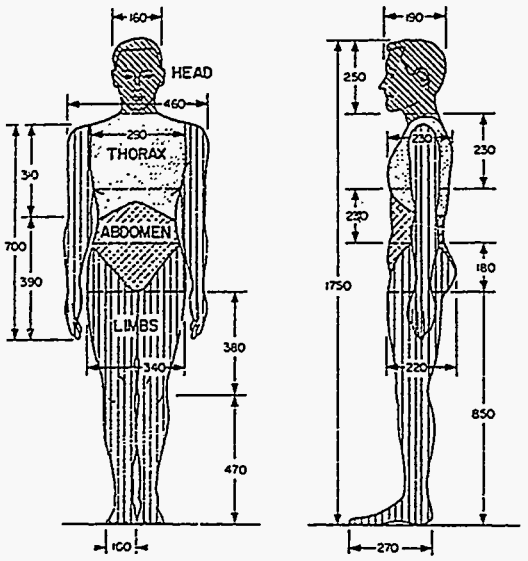

Figure 2.6: Sketch of a standard man.

Table 2.2: Area weightings for different body positions.

Body Position	Total Area Presented (ft^2)	Head A_{1j}	Thorax A_{2j}	Abdomen & Limbs A_{3j}
Standing	1.0	0.29	0.43	0.28
Sitting	2.9	0.10	0.14	0.76
Prone	5.1	0.09	0.23	0.68

Log-normal curves were fit to these composite curves by the method of maximum likelihood. The resulting log-normal curves are shown in Figure 2.7 along with a table listing the kinetic energy at 10, 50 and 90% probability of fatality and the log-normal parameters. The curves for the prone and sitting positions are nearly identical because the weighting of the body parts are very similar.

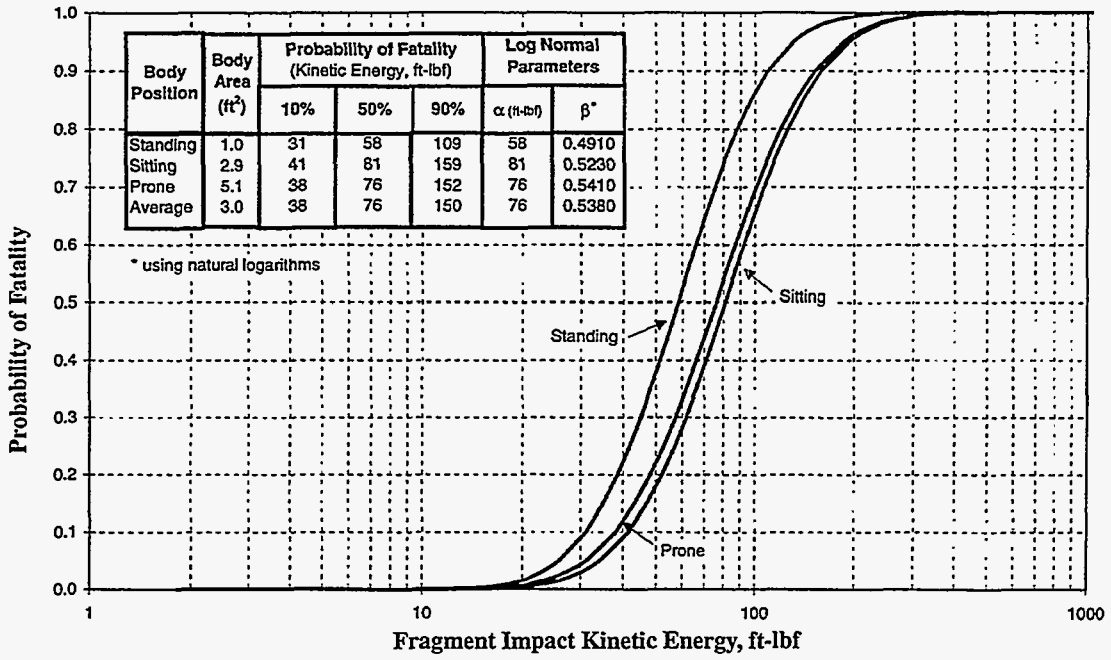

Body Position	Body Area (ft^2)	Probability of Fatality (Kinetic Energy, ft-lbf)			Log Normal Parameters	
		10%	50%	90%	α (ft-lbf)	β*
Standing	1.0	31	58	109	58	0.4910
Sitting	2.9	41	81	159	81	0.5230
Prone	5.1	38	76	152	76	0.5410
Average	3.0	38	76	150	76	0.5380

Figure 2.7: Probability of fatality from debris impacts for different body positions.

The probability of fatality for the three body positions was averaged assuming that equal numbers of the exposed population were standing, sitting, and prone. This average was weighted by the total body area presented by each position. The resulting curve is shown in Figure 2.8 as well as in Appendix A of the Standard 321-97.

The equation for achieving the average is:

$$\bar{P}(KE) = \frac{1}{\sum_{k=1}^{3} b_k} \left(\sum_{j=1}^{3} b_j P_j(KE) \right) \qquad (2.6)$$

where: P_j = probability of fatality due to fragment impact when in body position j,

b_j = total area presented by the body in position j, see column 2 of Table 2.2.

To calculate expected fatalities (E_F) from impact by a given debris' kinetic energy, it is necessary to multiply the probability of being struck by the probability of fatality. The probability of being

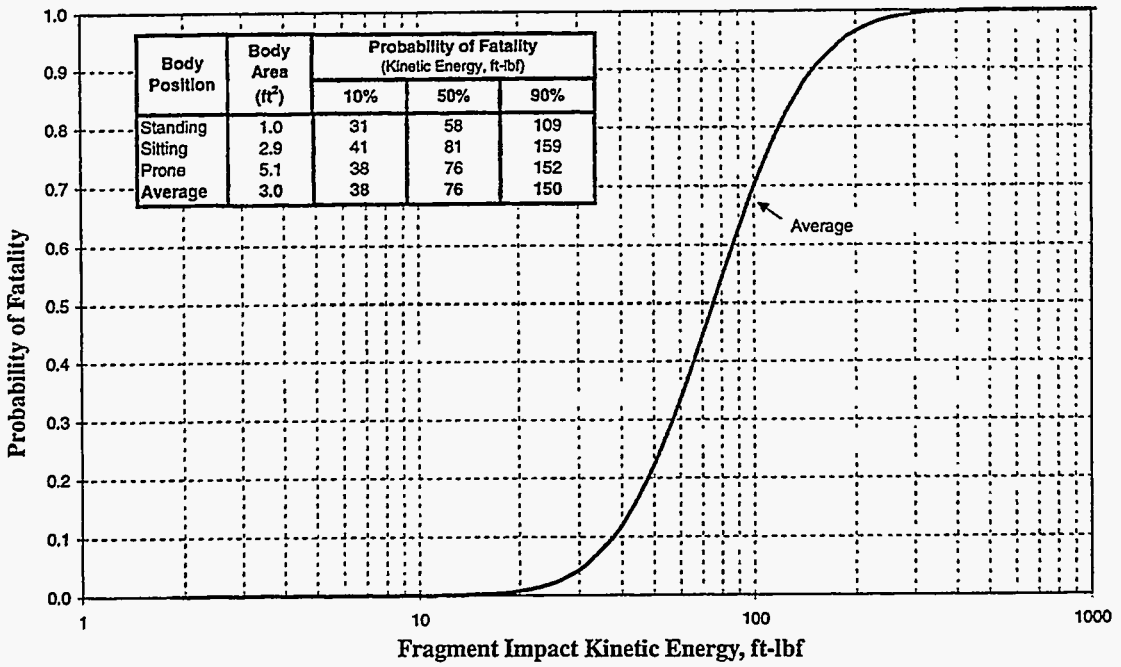

Figure 2.8: Average probability of fatality from debris impacts.

struck relates directly to the body's presented area. The prone position has a presented area that is more than five times the presented area for a standing person and nearly twice that for a seated person.

The angle that the falling debris makes with the vertical also affects the body's presented area. It is estimated that the majority of the impacts will be with debris falling almost vertically. However, it is possible through a combination of high winds, low ballistic parameter, and larger debris mass to have hazardous debris impacts at acute angles from the vertical that approach 90 degrees. If the larger presented area of the prone position is used, then regardless of the debris impact angle, a very conservative, E_F will result. Even when the impact area is a beach, this approach is conservative because many of the occupants will not be prone. In most cases where a majority of the people are prone, they will be within structures which provide considerably more protection from fragment impacts.

2.2 Other Studies Of Debris Impacts On People

There have been many studies into the effects of projectiles impacting the human body since the paper by Feinstein et al. A majority of this work has been sponsored by the U.S. Army Research Laboratory, USARL, at the Aberdeen Proving Ground, MD. The emphasis of most of these studies has been to understand the physiological effects of high velocity projectiles and weapon fragments and to quantify the physical capabilities lost by the person hit. Probability of fatality has not been a primary interest. An example of more recent studies is the information of Neades and Rudolph[28] on the probability of skin penetration and liver fracture which was presented at a DoD Explosive Safety Board (ESB) meeting in 1984. Figure 2.9 is a plot for skin penetration for

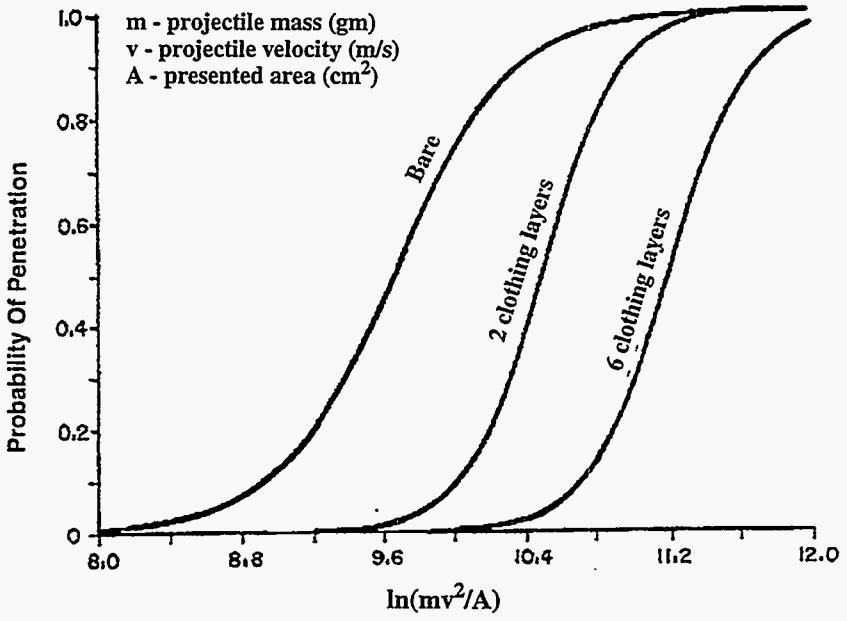

Figure 2.9: Probability curves for skin penetration.

the cases of bare skin, skin covered with two layers of warm weather military clothing, and skin covered with six layers of cold weather military clothing. Figure 2.10 is a plot for liver fracture. This study was performed by Edgewood Arsenal. Note that skin penetration is a function of the kinetic energy per unit of area presented by the fragment at impact and that liver fracture is a

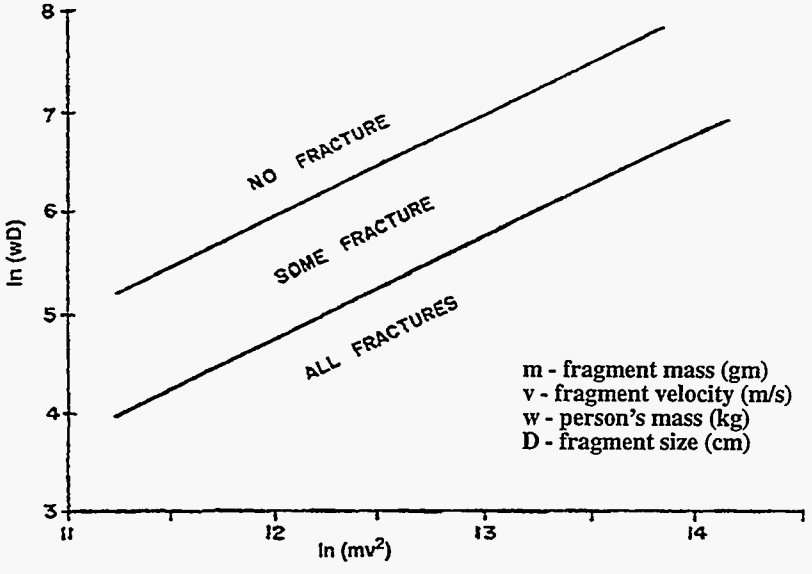

Figure 2.10: Blunt trauma liver fracture discriminant lines.

function of fragment kinetic energy. Also liver fracture depends upon the body mass, a larger body mass being less susceptible. This information is certainly applicable, but these types of data need to be assimilated by qualified analysts into a more usable form for the safety community. Table 2.3 applies the Neades and Rudolph's information to impacts by some common objects, originally characterized by Thomas Pfitzer of APT-Research Inc.

Fugelso, Weiner, and Schiffman[18] presented a paper in 1972 at an ESB meeting in which kinetic energy values for impacting fragments were stated for 10, 50 and 90% probability of fatality. These values were more conservative, i.e. lower energies, than those derived from the Feinstein et al study. Fugelso referenced Feinstein's work, but did not show how the stated energy values were obtained. These results were considered by the RALCT, but not used in the development of the S curves for this report. Table 2.4 contains the Fugelso et al recommendations.

Janser[21] also presented a paper in 1982 to the ESB on the lethality of fragments to unsheltered people. In it, he recommended log-normal curves for the probability of fatality from fragment impacts on four body parts: head, thorax, abdomen, and limbs. He based his study on Feinstein's work as well as more recent studies, but did not explain how his curves were generated. Table 2.5 contains the log-normal parameters for the curves he recommended. Compare the values of α and β in this table with those in figures 2.5 and it can be readily seen that Janser's fragment energy levels for a given probability of fatality are much greater than those recommended in the present study.

USARL has been developing a computer code called, "ORCA", for Operational Requirements-Based Casualty Assessment which is scheduled for beta release in 1997. It will be able to assess physical insults such as, blast overpressure, penetration, blunt trauma, abrupt acceleration, burns, toxic gases/agents, and electromagnetic energy. ORCA considers the orientation and position of a person relative to an incoming projectile as well as its mass, momentum and energy. It calculates the projectile's trajectory within the body and outputs the person's loss of mental and physical capabilities with time, assuming no medical attention for up to three days after the injury. This code or some derivative of it promises a means for improving the method presented here for evaluating the probability of fatality from fragment impact.

Table 2.3: Injury characteristics for some common objects.*

	Object Impacting	Mass (gm)	Velocity (fps)	Area (in^2)	Kinetic Energy (ft-lbf)	Probability of Bare Skin Penetration	Likelihood of Liver Fracture+
Terminal Velocity	Warhead Canister	2600	279	9.0	6936	1.000	Large
	Cable (6ft x 1 in)	1590	77	71.3	323	0.002	Some
	38 Cal. Bullet	16	432	0.11	102	1.000	Large
	30 Cal. Bullet	12	473	0.07	92	1.000	Large
	Warhead Fragment	70	174	0.62	73	0.966	Some
	Baseball	145	109	6.5	59	0.015	No
	Golf Ball	46	106	2.2	18	0.011	No
	22 Cal. Bullet	3	329	0.037	11	1.000	Some
	Penny	3	309	0.42	9.8	1.000	Some
	Nut & Bolt	14	93	0.44	4.1	0.018	No
Propelled	22 Cal. Bullet	3	1476	0.037	224	1.000	Large
	Golf Ball	46	249	2.2	98	0.632	Some
	90 mph Fast Ball	145	132	6.5	87	0.045	Some

* Probability of bare skin penetration and liver fracture based on data of Neades and Rudolph.[28]

+ Assuming a body mass around 68 kg (150 lbs).

Table 2.4: Energy levels associated with personnel injury from fragments, according to Fugelso et al.

Injury Level	Energy (ft-lbf)
Threshold	11
90% Injury (10% Fatal)	40
50% Injury (50% Fatal)	58
10% Injury (90% Fatal)	85

Table 2.5: log-normal fatality curves recommended by Janser.

Body Part	log-normal Parameters	
	α (ft-lbf)	β^*
Head	75	0.299
Thorax	173	0.591
Abdomen	214	0.425
Limbs	457	0.608

* Based on natural logarithms

Until more recent data on the effects of fragment impacts on people have been analyzed and assembled into a form readily used by safety personnel, it is recommended that the probability of fatality curves, Figures 2.7 and 2.8, be used to make the expected fatality calculations. The average log-normal curve can be used to make quick estimates of potential safety problems. When more detailed safety analyses are needed, statistics on the distribution of body positions can be used or credible assumptions made about the numbers of people standing, sitting, and prone. Then the more specific curves of Figure 2.7 can be used.

3 Debris Hazardous to Aircraft

A piece of debris is considered to be potentially lethal to an aircraft if it is capable of producing sufficient damage to cause loss of life or necessitate emergency response by the crew to avoid a catastrophic consequence. The two principal ways that debris can be hazardous to aircraft are: (a) fragment penetration of a critical aircraft structure or the windshield and (b) fragment ingestion by an engine.

3.1 Fragment Penetration

Business jets are more at risk from fragment penetration than other classes of aircraft, because they fly relatively fast and are constructed of relatively thin materials. For a jet aircraft cruising at 450 kts and 50,000 ft, the relative velocity between the aircraft and a 10 mm-diameter, solid steel spherical fragment in terminal velocity is about 830 fps.

Initially, a study was made using the THOR equations[38, 39] to determine the size fragments that could penetrate wing leading edges and windshields. These empirical equations were developed by the Ballistics Analysis Laboratory of Johns Hopkins University for the U.S. Army Ballistic Research Laboratory. However, goodness of fit information published in reference 38, indicated that the THOR empirical equations had standard deviations in residual velocities greater than 350 fps for steel and aluminum projectiles impacting aluminum targets. These translate into predictive uncertainties for the THOR equations as great as $\pm$ 50-100% when the impact speed range of interest is less than 1000 fps.

The recently completed penetration code, FATEPEN2,[40, 41] was subsequently obtained from the Naval Surface Warfare Center (NSWC), Dahlgren, VA. It is being used at NSWC to evaluate the vulnerability of aircraft to impacts by high speed fragments from various types of warheads. Inquiries were made concerning this code's predictive accuracy. The code developers provided several plots which showed that the empirical equations fit experimental penetration data for Lexan, Kevlar, and fiberglas reasonably well down to impact speeds below 1000 fps. No overall accuracies were stated for the code. Note that the experimental data used to develop the THOR equations were a subset of the data used to develop the FATEPEN2 equations.

Table 3.1 compares the penetration predictions of the THOR and FATEPEN2 equations for impacting solid spherical fragments. Windshields typically used for light aircraft were assumed to be one piece constructions of Lexan, cast acrylic, stretched acrylic, or bullet resistant glass, 0.50 inch thick with a 40^{o} rearward rake. The impact velocity was set at 800 fps. FATEPEN2 predicts that larger fragments are required to penetrate plastic windshield materials than THOR. For aluminum and glass targets, FATEPEN2 predicts that smaller steel fragments are required.

Short solid cylinders impacting end-on are more effective penetrators than solid spheres of the same diameter because of their greater mass to presented area. Table 3.2 presents only FATEPEN2 predictions for solid, short, cylindrical fragments, L/D~1 of aluminum, steel and tungsten, penetrating a 0.06 inch thick leading edge or a 0.5 inch thick windshield. Aircraft windshields were generally predicted to be more resistant to penetration than wing leading edges.

Table 3.1: Comparison of THOR and FATEPEN2 penetration predictions.

Target			Smallest Penetrating Solid Spherical Fragment THOR/FATEPEN2		
Material	Thickness (in)	Rake Angle (deg)	Material	Diameter (mm)	Mass (gm)
Aluminum	0.06	0	Steel	5/3	0.5/0.1
	0.06	0	Aluminum	12/18	2.4/8.7
Lexan	0.50	40	Steel	3/23	0.1/46.7
	0.5	40	Aluminum	10/49	1.4/168.5
Cast Acrylic	0.5	40	Steel	8/20	2.1/34.3
	0.5	40	Aluminum	23/34	16.8/58.0
Stretched Acrylic	0.5	40	Steel	3/20	0.1/34.3
	0.5	40	Aluminum	18/34	8.1/58.0
Bullet Resistant Glass	0.5	40	Steel	11/10	5.1/4.0
	0.5	40	Aluminum	28/13	30.4/3.3

The 0.09 gm steel fragment predicted to penetrate a 0.06 inch (0.15 cm) aluminum leading edge is impractically small for range safety to have to consider. So light aircraft construction was examined in more detail. Figure 3.1 shows a typical light aircraft front wing section. A penetrating fragment would encounter, at a minimum, the leading edge, a baffle, and the front wing spar, all constructed of aluminum with thickness of about 0.05, 0.025 and 0.071 inches, respectively. The space in the forward portion of the wing could also contain tubing for a warm air deicing system, but critical components, such as hydraulic lines, electrical cables, or control mechanisms, are usually not located there. It is undesirable for a fragment to penetrate the leading edge and the baffle, but significant damage could result from a fragment actually penetrating the front wing spar which normally forms one wall of a fuel tank. Table 3.3 shows the smallest fragments that FATEPEN2 predicts could penetrate the leading edge, baffle and front wing spar of a light aircraft wing to puncture the fuel tank. These fragments are assumed to be a short solid cylinders, L/D~1. If the debris does not contain very dense fragments like tungsten, the smallest fragment mass for concern is 1.9 gm. The predicted aluminum fragment mass is much larger than for the steel or tungsten. Since aluminum has lower mechanical strength it tends to mushroom in shape much more during impact. This greatly increases the fragment area presented for impact and the mass required for penetration.

Table 3.2: FATEPEN2 predictions of smallest penetrating fragment.

Target			Smallest Penetrating Fragment*		
Material	Thickness (in)	Rake Angle (deg)	Material	Size (mm)	Mass (gm)
Aluminum	0.06	0	Aluminum	10.7	2.7
	0.06	0	Steel	2.4	0.09
	0.06	0	Tungsten	1.9	0.09
Steel	0.06	0	Aluminum	16.1	9.1
	0.06	0	Steel	10.1	6.3
	0.06	0	Tungsten	7.1	4.9
Lexan	0.50	40	Aluminum	36.1	102.3
	0.50	40	Steel	16.6	28.1
	0.50	40	Tungsten	9.2	10.6
Cast & Stretched Acrylic	0.50	40	Aluminum	27.9	47.2
	0.50	40	Steel	16.6	28.1
	0.50	40	Tungsten	11.2	19.1
Bullet Resistant Glass	0.50	40	Aluminum	11.8	3.6
	0.50	40	Steel	8.9	4.3
	0.50	40	Tungsten	7.2	5.1

* Fragments are short solid cylinders (L/D~1) impacting end-on.

Table 3.3: FATEPEN2 predictions for penetration of light aircraft wing front section.

Target		Smallest Penetrating Fragment*		
Material	Rake Angle (deg)	Material	Size (mm)	Mass (gm)
Aluminum	0	Aluminum	20.9	19.8
Aluminum	0	Steel	6.8	1.9
Aluminum	0	Tungsten	3.1	0.4

* Fragments are short solid cylinders (L/D~1) impacting end-on.

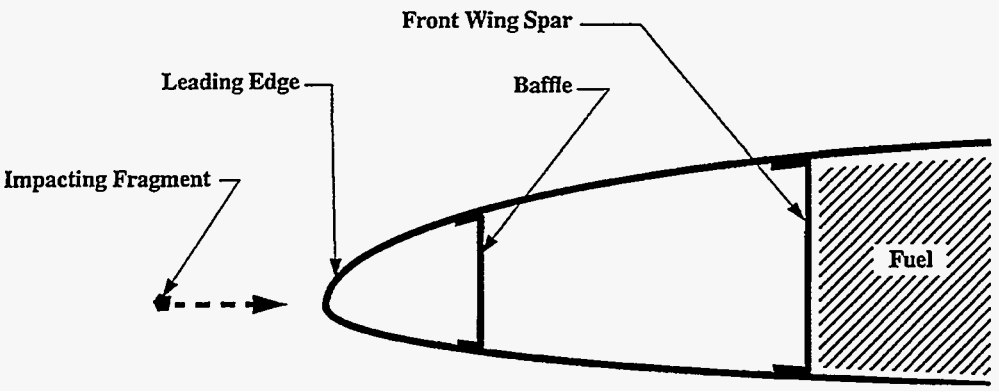

Leading edge, baffle, and spar are assumed to be constructed of 0.05, 0.025 and 0.071 inch thick aluminum, respectively.

Figure 3.1 Typical construction of an aerodynamic structure for a light aircraft.

3.2 Fragment Ingestion By An Aircraft Engine

Aircraft and helicopters flying in a region through which debris is falling could possibly ingest fragments into their engines. Piston engines were considered, but were not pursued because their physical construction with intake filters and manifolding make it difficult for fragments to get inside to affect moving parts. Debris clogging the air filters can become a serious problem when flying through an extensive cloud of volcanic dust, but should not be a problem with debris from a missile test.

Aircraft gas turbine engines can be divided into three categories: turbojet, turboshaft and turbofan.[43] Only a part of the air processed through a turbofan engine actually goes through the engine core which contains the compressors, burners and turbines. The rest passes only through the fan. The ratio of the air mass passed through the fan to that passed through the core is defined as the "bypass ratio". Turbojet and turboshaft engines have zero bypass ratios. Turbofan engines can have bypass ratios up to and exceeding eight.

Any fragment ingested into an engine with zero bypass will have to pass through the engine core, if it does not become lodged somewhere within the engine. In turbofan engines, an ingested fragment is likely to be centrifuged outward to pass only through the fan and not enter the engine core. The greater the bypass ratio, the smaller, the chance that a fragment will enter the engine core.

Engine damage can result from solid fragment ingestion, almost independently of the fragment's relative speed. Damage is primarily a function of the fragment's physical size and mechanical strength relative to those of the engine's compressor blade materials. Material density which exerts so much influence in penetration is of secondary importance for ingestion. It is reasonable to expect an engine to tolerate larger aluminum than steel fragments and about the same size tungsten fragments since their tensile strengths are, respectively, less than and about the same as steel

One of the worst objects that an engine can ingest is a piece of cloth, e.g. a shop rag. When ingested, a rag can become entangled between rotor and stator blades causing them to bend and interfere. The rag when caught on the face of a rotor or stator can also disrupt the air flow through the engine causing a stall or flameout. Thin plastic sheets and quilted pads sometimes used on missile and space vehicles for thermal protection could become part of the falling debris and act somewhat like a rag if ingested.

Thus, a low, slow flying airplane or helicopter can be at risk as well as a high, fast flying one. A more important parameter for ingestion hazards is the size of the engine. Smaller engines tend to be more vulnerable to fragment ingestion than larger ones. Also, engines with axial flow compressors tend to be more vulnerable than those with centrifugal compressors.

The Federal Aviation Administration requires manufacturers of gas turbine engines to demonstrate through testing that their engines can withstand ingestion of prescribed masses of birds, ice, and sand. There is no requirement for ingestion tests of other foreign objects and, consequently, the information is sparse and mostly anecdotal.

The U.S. Army Research Laboratory (ARL), has overviewed foreign object ingestion by military aircraft for a number of years.[44, 45] They consider some of the smaller turboshaft engines with axial flow compressors to be the most vulnerable to foreign object ingestion. Such engines power some small aircraft and small helicopters. Personnel at ARL estimate that engine damage could occur if one of these small engines ingested a 1-gram compact fragment of steel or tungsten. A somewhat larger compact fragment mass of aluminum would be required to cause the same damage because it is mechanically weaker and less dense. At this time there is no experimental data to confirm this.

Table 3.4 provides a list of the smallest fragments masses that can be potentially lethal to the more vulnerable aircraft and helicopters. If there are no high density fragments, e.g., tungsten, it is recommended that one gram be used as the smallest fragment mass that can be potentially lethal to an aircraft from structural penetration or engine ingestion.

Table 3.4: Smallest potentially lethal fragments for aircraft.

Event	Fragment Material	Smallest Fragment Mass (gm)
Penetration of Structure or Windshield	Aluminum	3.5
	Steel	2.0
	Tungsten	0.5
Engine Ingestion	Aluminum	> 1
	Steel	~1
	Tungsten	< 1

3.3 Debris Encounter Model

A study was made to assess the magnitude of the probability that an aircraft would encounter a piece of debris. An exoatmospheric intercept between an incoming target missile and an interceptor was modeled with the debris generation model, FASTT[49] which was developed by Kaman Sciences through the sponsorship of the Defense Nuclear Agency. NASA, the U.S. Air Force and the U.S. Army have also developed computer models for predicting debris generation for various events, e.g., hypervelocity impact, and explosive disassembly. Only fragments that were 10 mm or greater in size were considered in this example, to limit the number of fragment trajectories that had to be calculated. Still, FASTT predicted the generation of more than 20,000 fragments. Figure 3.2 presents a spacial model for falling debris from an exoatmospheric event assuming no atmospheric wind. In this example, the debris was monitored over time in six annular regions. At one second intervals a count was made of the number of fragments that occupied each annular region between the altitudes of 40 and 50 kft. It was assumed that the fragments were uniformly distributed within each region. Figure 3.3 shows the number density for the different regions versus time from the debris generating event. Aircraft were assumed to be flying straight and level at cruise speed and a constant altitude of 45 kilofeet and to pass through the debris cloud when the fragment number densities were near their maximum. Figure 3.3 shows Flight A passing directly through the center of the debris cloud and Flight B skirting all, but the outermost region. The cross sectional area of each aircraft was approximated by multiplying its wingspan by its overall height, designated here as the maximum frontal area, A_{front}.

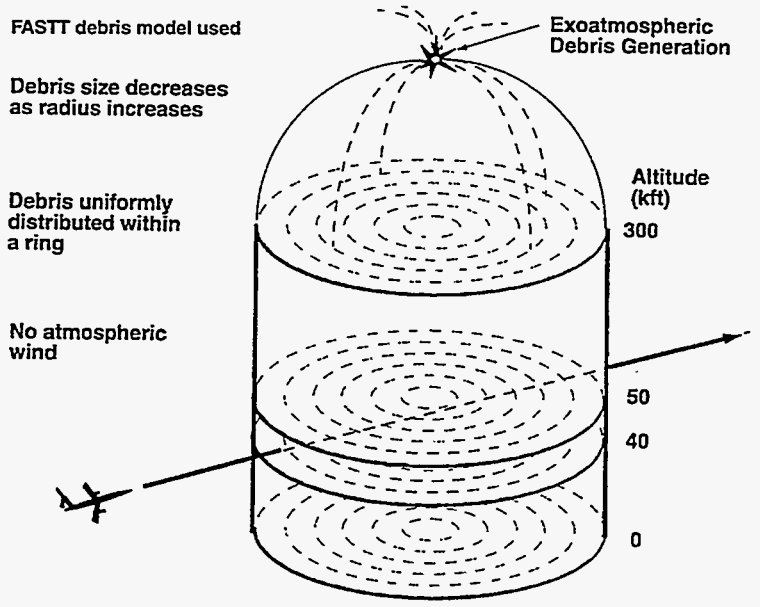

Figure 3.2: Simple model of space through which debris falls.

The probability of fragments impacting an aircraft, P_I, was calculated using the equation:

$$P_I = A_{front} \sum_{i=1}^{K_R} S_i N_i \tag{3.1}$$

where: S_i = distance aircraft travelled in passing through annular region i,

N_i = fragment number density in annular region i at time $\bar{t}_i$,

$\bar{t}_i$ = average of entering and exiting time for annular region i,

K_R = number of annular regions flown through, (for Flight A, $K_R = 11$).

Table 3.5 presents the results for a Lear Jet and a Boeing 747. A more refined estimate of the aircraft cross sectional area would decrease the probability of impact.

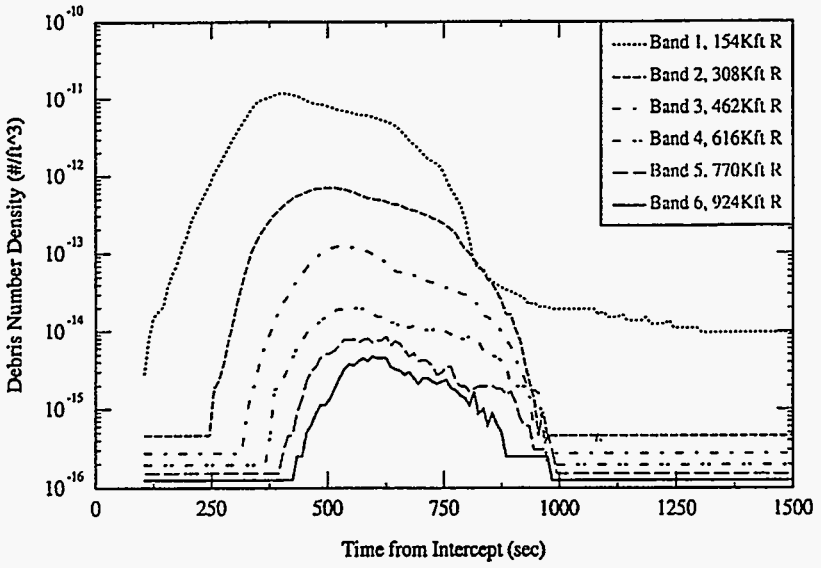

Figure 3.3: Temporal number density of debris between the altitudes of 40 and 50 kilofeet for various annular spaces (bands).

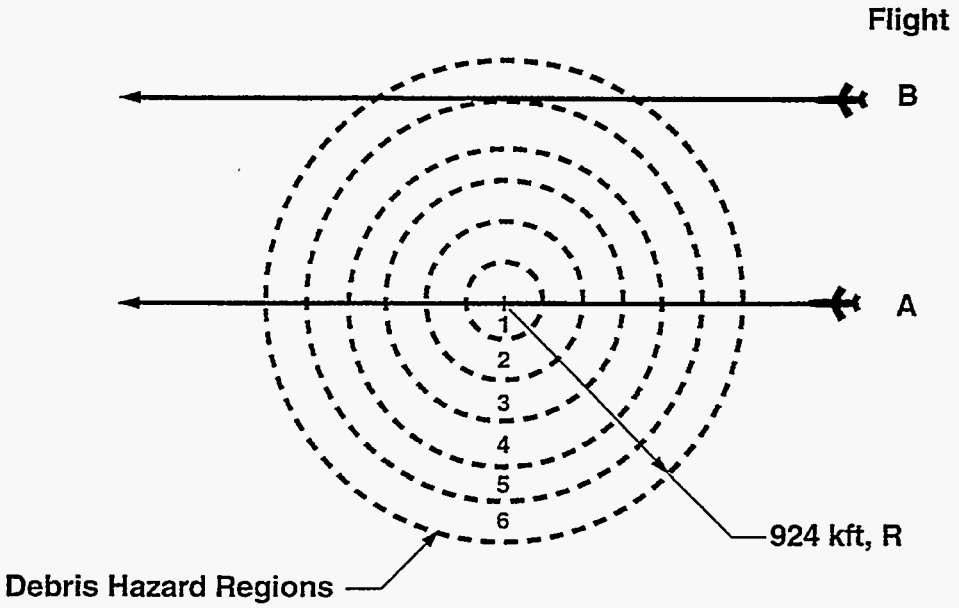

Figure 3.4: Aircraft trajectories through the debris space.

Table 3.5: Results for two sample flights through debris encounter model.

	Time From Debris Generation (sec)			Probability Of Debris Impact	
Flight	Enters Outer Region	Nearest The Center	Exits Outer Region	Lear 35A	Boeing 747
A	-592	625	1843	7.1×10^{-4}	1.8×10^{-2}
B	-47	625	1297	4.9×10^{-7}	1.2×10^{-5}

3.4 Engine Capture Area

When a propeller or jet propelled aircraft is flying subsonically, its engines draw air from an upstream region whose cross sectional area is greater than the actual area of the engine inlet. Figure 3.5 illustrates this effect.

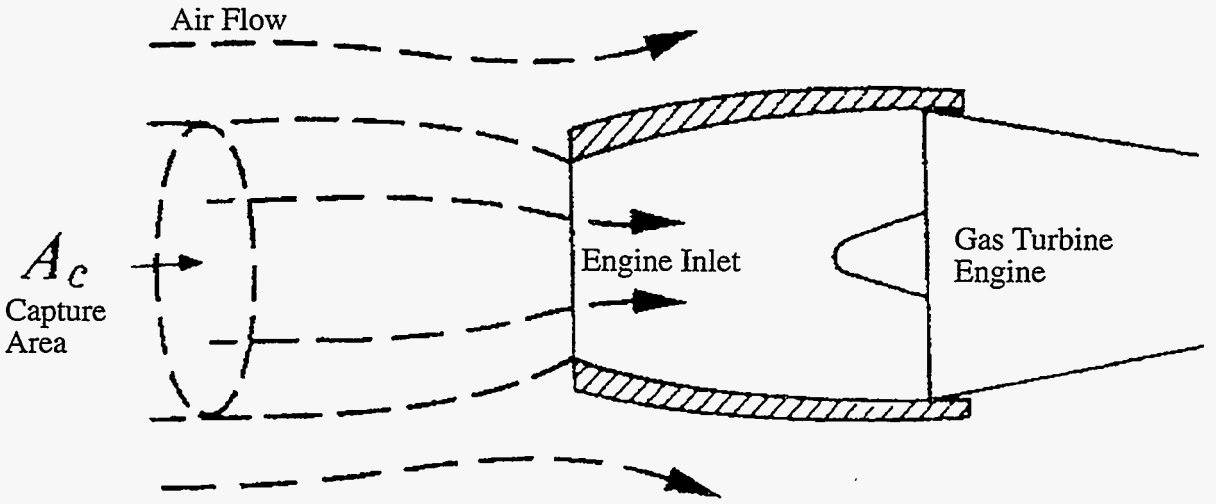

Figure 3.5: Schematic of subsonic air flow into engine inlet.

The equation for the larger upstream area, the capture area, from which air is drawn by a propeller[46] is:

$$\frac{A_C}{A_{prop}} = 1 + \left(\frac{T}{2\rho_\infty V_\infty{}^2 A_{prop}} \right)^{\frac{1}{2}} \qquad (3.2)$$

where: A_C = capture area

A_{PROP} = propeller area

V_∞ =aircraft velocity

ρ_∞ = density at cruise altitude

T = engine thrust

The effective capture area for an inlet of the engine powering the propeller can be approximated by multiplying the inlet area by this ratio determined for the propeller.

For a turbojet or turbofan aircraft,[47] the equation for the capture area is:

$$A_C = \frac{\dot{m}_E}{\rho_\infty V_\infty} \left(1 + \frac{\dot{m}_S}{\dot{m}_E} \right) \qquad (3.3)$$

where: $\dot{m}_E$ = engine mass flow rate

$\dot{m}_S$ = secondary mass flow rate for engine cooling, ejector air.

Typical $\frac{\dot{m}_S}{\dot{m}_E} = \begin{bmatrix} 0.2 & \text{fighter} \\ 0.03 & \text{transport} \end{bmatrix}$

Table 3.6 lists a range of capture area ratios for various types of aircraft.

To determine the probability of debris being ingested by an engine of a Lear 35A or Boeing 747 aircraft when flying through the example debris cloud on trajectory A or B, the ratio, A_C/A_{front}, for the aircraft type is multiplied by the probability of debris impact listed in Table 3.5. So, the probabilities of ingestion of at least one piece of debris by the Lear 35A and Boeing 747 on trajectory A are 2.8×10^{-5} and $7.2 \times 10,^{-4}$ respectively. On trajectory B, they are 2.0×10^{-8} and $4.8 \times 10,^{-7}$respectively.

In summary, steel fragments as small as 2 gm and tungsten as small as 0.5 gm could be a penetration hazard to aircraft. Steel or tungsten fragments as small as 1 gm could be an ingestion hazard for the smallest gas turbine engines. Aluminum being mechanically weaker and less dense is not a hazard in these small masses.

Table 3.6: Area Parameters for different aircraft classes.

Type	Cruise Speed (fps)	Inlet Area per Engine (ft^2)	Maximum Frontal Area, A_{front} (ft^2)	Total Capture Area, A_C (ft^2)	A_C/A_{front}
Commercial Turbofan	700-800	40-45	8000-14000	250-450	0.02-0.04
Business Turbofan	700-800	4-5	450-650	14-18	0.02-0.04
Military Turbofan	700-950	5-7	500-600	15-25	0.03-0.04
Turboprop	300-520	0.4-2.2	700-5000	0.5-11	0.001-0.002
Helicopter Turboshaft	170-200	1.5-3	300-500	2-4	0.006-0.008

The low probability of impact and ingestion results calculated for a worst case trajectory through a debris cloud suggest that these risks may be satisfactorily managed through small modification to the timing and routing of commercial and privates flights.

4 Debris Hazardous to Ships or Boats

Falling inert debris can be hazardous to the occupants of a ship or boat in two ways. A fragment can directly impact a person exposed on the deck or it can penetrate the structure and cause problems below deck that could lead to the ship or boat being seriously damaged or destroyed. The concerns for an exposed person onboard are the same as for an exposed person on land and have already been addressed. Fragment impacts on a ship or boat are addressed here.

4.1 FATEPEN2 Penetration Predictions

A potentially lethal fragment for a ship or boat was defined as one which can penetrate a deck or weather covering. The FATEPEN2 code[40, 41] was used to quantify the sizes of aluminum, steel, and tungsten fragments which could just penetrate decks made of 0.25 inch thick aluminum, steel, or Doron, or 0.50 inch thick oak. Doron is a laminated panel made from bonded woven-roving fiberglass. The material thicknesses used in the calculations are those more typically found on smaller ships and pleasure craft, e.g. sailboats. Note that sailboat decks are frequently constructed of 0.50 inch thick balsa wood laminated between 0.12 inch thick fiberglass. If no penetration strength is assumed for the balsa wood this deck can be represented in FATEPEN2 calculations as 0.25 inch thick fiberglass. Each fragment was assumed to be a compact solid cylinder with L/D~1 falling in a tumbling mode at its terminal velocity for sea level conditions.

The FATEPEN2 calculations indicate that penetration of 0.25 inch fiberglass requires the least fragment mass for aluminum and steel fragments, that is 14 and 5 kg, respectively. While the smallest mass of tungsten, 0.4 kg, is defined by the penetration of 0.25 inch aluminum. Table 4.1 presents these results which are assumed to have an uncertainty of $\pm$50%.

If mission essential ships all have steel decks and high density materials like tungsten are not present in significant quantities in the debris, then range safety can make probability of impact calculations considering only fragments with mass greater then 6 kg. If high density materials are present, fragments with mass down to 3 kg must be considered.

For non-mission essential watercraft with no high density materials present in the debris, fragments with mass down to 5 kg must be considered. If high density materials are present, it will be necessary to included fragments with mass down to 0.4 kg.

4.2 Stanford Equation

The fragment velocities required for deck penetration are mostly below those of the penetration data that was used to develop the empirical penetration equations used in FATEPEN2. Thus, a second independent predictive method was sought. The Stanford equation[42] was reported to give reasonable predictions of penetration of steel and concrete by steel missiles in the velocity range of interest.

The equation is:

$$\frac{E}{D} = \frac{S}{46,500}\left(16,000T + 1,500\frac{W}{W_S}T\right) \qquad (4.1)$$

where: E = critical kinetic energy required for perforation (ft-lbf),
D = missile or fragment diameter (inches),
S = ultimate tensile strength of the target (steel plate) (psi),
T = target plate thickness (inches),
W = length of a square side between rigid supports (inches),
W_S = length of a standard width (4 inches)

Note that this equation takes into account the distance between the supports of the target plate. FATEPEN2 does not.The range of applicability for this equation is:

$$0.1 < T/D < 0.8$$
$$0.002 < T/L < 0.05$$
$$10 < L/D < 50$$
$$5 < W/D < 8$$
$$8 < w/T < 100$$
$$70 < V_C < 400$$

FATEPEN2 predicted that a 6.35 kg (14 lbm) steel fragment, D = 4 in., falling with a terminal velocity of 320 fps could just penetrate a 0.25 inch thick steel plate. Assuming W = 24 in. and S = 110,000 psi, the Stanford equation predicts that this fragment will require a velocity of 375 fps. In this particular case the results from the two methods compare reasonably well, differing by only 17% in velocity. However, T/D, L/D and W/D were all below the stated range of applicability for the Stanford equation.

These penetration predictions need to be revisited when applicable experimental data and/or better predictive equations become available.

Table 4.1: Smallest debris fragment that can penetrate deck materials.

Target		Smallest Penetrating Fragment*	
Deck Material	Thickness (inch)	Fragment Material	Mass (kilograms)
Aluminum	0.25	Aluminum	15
	0.25	Steel	5
	0.25	Tungsten	0.4
Steel	0.25	Aluminum	17
	0.25	Steel	6
	0.25	Tungsten	3
Doron (Fiberglass)	0.25	Aluminum	14
	0.25	Steel	5
	0.25	Tungsten	2
Oak	0.50	Aluminum	66
	0.50	Steel	23
	0.50	Tungsten	2

* Fragment is a short solid cylinder, L/D~1. impacting end-on.

5 Summary and Recommendations

- Log-normal curves which relate the impact kinetic energy of a fragment to the probability of fatality have been developed for people in standing, sitting, and prone positions. An average curve was also calculated assuming equal numbers of people in the three positions. It showed that a fragment kinetic energy of 76 ft-lbf would have a 50% probability of killing the person struck. The physiological basis for these curves was obtained from studies reported in 1968 by Feinstein et al. Results from other investigators were also presented.

- It is recommended that the log-normal curves presented in this report be used by range safety analysts until better predictive tools become available. The average log-normal curve can be used to make quick estimates of potential safety problems. When more detailed safety analyses are done, statistics on the distribution of body positions can be used or credible assumptions can be made about the numbers of people standing, sitting, and prone in the debris fall area. Then the curves specific to those body positions can be used.

- Steel fragments as small as 2 gm and tungsten as small as 0.5 gm could represent a penetration hazard to aircraft. Steel or tungsten fragments as small as 1 gm could be an ingestion hazard for the smaller gas turbine engines. Aluminum, being mechanically weaker and less dense, is not a hazard in these small masses.

- The low probability of impact and ingestion results calculated for a worst case trajectory through a debris cloud suggest that aircraft risks may be satisfactorily controlled with only small changes in timing and routing of commercial and privates flights.

- If mission essential ships have steel decks and high density materials, like tungsten, are not present in significant quantities in the debris, then range safety can make probability of impact calculations considering only fragments with mass greater then 6 kg. If high density materials are present, fragments with mass down to 3 kg must be considered.

- For non-mission essential watercraft with aluminum or fiberglass decks, fragments with mass down to 5 kg must be considered when no high density materials are in the debris. If high density materials are present, it will be necessary to included fragments with mass down to 0.4 kg.

- The considerable physiological data base that currently exists concerning impacts on people needs to be assimilated by qualified analysts into a form readily used by the safety community.

- Fragment penetration prediction methods need to be further developed and validated for the lower impact velocity regime, < 300 m/s.

- A data base on the effects of debris ingestion by gas turbine engines needs to be greatly expanded.

6 Bibliography

Impact Hazards To People

1. *Abstracts of the Explosive Safety Seminars 1959-1992*, AD-A302396.

2. Ahlers, Edward B., *Debris Hazards, a Fundamental Study*, Report No. DASA-1362, IIT Research Institute, June 1, 1966.

3. Ahlers, Edward B., *Fragment Hazard Study,* IIT Research Institute, Chicago, IL, Presented at the Armed Services 11th Explosive Safety Seminar, September 1969, AD-862 868.

4. Ahlers, E. B., *Fragment Hazard Study*, Minutes of the 11th Explosive Safety Seminar, Vol. 1, Armed Service Explosives Safety Board, Washington, DC, September 1969.

5. Ahlers, E. B., *Fragment Hazard Study (U),* ITT Research Institute, Lanham, MD, September 1969, AD-A956 255.

6. *Air to Surface Target Vulnerability,* Book 1 of 2, JTCG/ME 61A1-3-9 (U.S. Army FM 101-50-19), Joint Munitions Effectiveness Manual (JMEM), November 1979.

7. *A Manual for the Prediction of Blast and Fragment Loadings on Structures*, DOE Albuquerque Operations Office, Februáry 1992.

8. Beverly, William B., *A Human Ballistic Mortality Model,* U.S. Army Ballistic Research Report ARBRL-TR-02088, Aberdeen, MD, July 1978.

9. Beverly, William B., *A Monte Carlo Solution of the Human Ballistic Mortality Model,* U.S. Army Ballistic Research Report ARBRL-TR-02098, Aberdeen, MD, August 1978.

10. Clemenson, C. J., Hellstrom, G. and Lingren, S., *The Relative Tolerance of the Head, Thorax, and Abdomen to Blunt Trauma,* Annuals of the New York Academy of Sciences, Vol. 152, Art. 1, pp. 187+, October 1968.

11. Dziemian, A. J., *A Provisional Casualty Criterion for Fragments and Projectiles,* CWLR 2391, May 1960.

12. Fackler, Martin L., MD, *Wound Ballistics, A Review of Common Misconceptions*, Journal of the American Medical Association, Vol. 259, No. 18, May 13, 1988.

13. Feinstein, D. I., Haugel, W. F., Kardatzke, M. L., and Weinstock, A., *Personnel Casualty Study*, Illinois Institute of Technology Research Institute Project No. J6067, July 1968, AD 842 573.

14. Feinstein, D. I., Nagaoka, H. H., *Fragmentation Hazards to Unprotected Personnel,* IIT Research Institute, Chicago, IL, Presented at the Armed Services 13th Explosives Safety Seminar, September 1971, AD 890 544.

15. Feinstein, D. I., *Fragment Hazard Criteria,* IIT Research Institute, Chicago, IL, Presented at the Armed Services 13th Explosive Safety Seminar, September 1971.

16. Feinstein, D. I., *Fragmentation Hazard Evaluations and Experimental Verification,* IIT Research Institute, Chicago, IL, Presented to the Armed Services 14th Explosive Safety Board, November, 1973.

17. Feuchtwanger, Moshe M., MD, FACS, *High Velocity Missile Injuries: A Review,* The Royal Society of Medicine, Vol. 75, December 1982.

18. Fugelso, L. M., Weiner, L. M., and Schiffman, T. H., *Explosive Effects Computation Aids,* Final Report GARD Project No. 1540, General American Research Division, General American Transportation Corp, Niles, IL.

19. Gurdjian, E. S., J. E. Webster and H. L. Lissner, *Studies on Skull Fracture with Particular Reference to Engineering Factors,* Amer. J. Surg., 78: 736-742, 1949.

20. Hill, B. D. and Mills, J., *Personnel Injury Probability: Human Vulnerability To Inert Debris,* TYBRIN Corporation Report TYBRIN-40-29000, April 1997.

21. Janser, P. W., *Lethality of Unprotected Persons due to Debris and Fragments,* Prepared for presentation at the Armed Services 20th Explosive Safety Seminar, August 1982.

22. Katz, B. S. and Egner D. O., *Los Angles County District Attorney's Less-Lethal Weapons Task Force,* U.S. Army Human Engineering Laboratory, Aberdeen Proving Ground, MD, June 1976.

23. Kokinakis, W., *A Note on Fragment Injury Criteria,* U.S. Army Ballistic Research Lab, Aberdeen, MD, Presented at the Armed Services 13th Explosives Safety Seminar, September 1971, AD 890 544.

24. Kokinakis, W., *A New Methodology for Wounding and Safety Criteria,* Proceedings of the Armed Services 16th DDESB Explosive Seminar, September 1974, pp. 1209-1226.

25. McCleskey, Frank, *Drag Coefficients for Irregular Fragments,* Naval Surface Weapons Center, Dahlgren, VA, August 1986, AD P005 364.

26. McCleskey, F., Neades, D. N., Rudolph, R. R., *A Comparison of Two Personnel Injury Criteria Based on Fragmentation,* Kilkeary Scott and Associates Inc, King George, VA, AD A235005. Presented at the Explosives Safety Board Meeting, August, 1990.

27. McMillan, J. H. and Gregg, J. R., *The Energy Mass and Velocity Which is Required to Produce a Casualty*, OSRD Missile Casualty Report No. 12, November 1945.

28. Neades, D. N. and Rudolph, R. R., *An Examination of Injury Criteria for Potential Application to Explosive Safety Studies*, Prepared for presentation to the Explosive Safety Board (DDESB) in 1983-84.

29. Rich, Norman M., MD, FACS, COL, MC, USA, *Missile Injuries*, The American Journal of Surgery, Vol. 139., March 1980.

30. Richmond, D. R., Yelverton, J. T., Fletcher, E. R., *New Airblast Criteria for Man*, Los Alamos National Laboratory, Los Alamos, NM, Presented at the 22th Explosives Safety Seminar, August 1986.

31. Rudolph, R. R., *Fragment Injury Criteria Investigation (U)*, Ketron, Inc. Report No. KFR 469-84 for the US Army Ballistic Research Laboratory, February 1984.

32. Sperrazza, J. and Kokinakis, W., *Ballistic Limits of Tissue and Clothing*, Technical Note No. 1645, Army Ballistic Research Laboratories, RDT&E Project No. 1P025601A027, Ballistic Research Laboratories, January 1967.

33. Swan, Kenneth G., COL, MC USAR, Reiner, Dan S., MD, and Blackwood, James M., MD, *Missile Injuries: Wound Ballistics and Principles of Management,* Military Medicine, Vol. 152, January 1987.

34. Wargovich, M. J., Egner, D. O., Busey, W. M., Thein, B. K., and Shank, E. B., *Evaluation of the Physiological Effects of a Rubber Bullet, a Baseball, and a Flying Baton,* U.S. Army Human Engineering Laboratory, Aberdeen Proving Ground, MD, September 1975.

35. White, C. S., *The Nature of the Problems Involved in Estimating the Immediate Casualties from Nuclear Explosions,* CEX-71.1. Civil Effects, U.S. Atomic Energy Commission, DR-1886, July 1971.

36. Zaker. T. A., Lauer, J., Feinstein, D. I., and Ahlers, E. B., *Fragmentation Hazard Study, Phases I and II,* IIT Research Institute Final Report, April 1970, Contract DAHC-04-69-C-0056, AD-869009.

37. Zaker, T. A., *Fragment and Debris Hazards,* Technical Paper No. 12, Department of Defense Explosives Safety Board, July 1975, AD-A013 634.

Fragment Penetration

38. Ballistic Analysis Laboratory, Johns Hopkins University, *A Comparison of the Performance of Fragments of Four Materials Impacting on Various Plates (U),* Baltimore, Institute for Cooperative Research, May 1959, (Project THOR, Technical Report No. 41).

39. Ballistic Analysis Laboratory, Johns Hopkins University, *The Resistance of Various Non-Metallic Materials to Perforation by Steel Fragments: Empirical Relationships for Fragments Residual Velocity and Tesidual Weight (U),* Baltimore, Institute of Cooperative Research, BAL/JHU, April 1963, (Project THOR, Technical Report No. 51.)

40. Yateau, J. D., Zernow, R. H., and Recht, R. F., *Compact Fragment Multiple Plate Penetration Model (FATEPEN2) Volume 1 - Model Description,* Applied Research Associates, Inc., prepared for the Naval Surface Warfare Center, Dahlgren, VA, January 1991.

41. Yateau, J. D., Zernow, R. H., and Recht, R. F., *Compact Fragment Multiple Plate Penetration Model (FATEPEN2) Volume 2 - Computer Code User's Manual,* Applied Research Associates, Inc., prepared for the Naval Surface Warfare Center, Dahlgren, VA, January 1991.

42. Gwaltney, R. C., *Missile Generation and Protection in Light-Water-Cooled Power Reactor Plants*, ORNL, NSIC-22, Oak Ridge National Laboratory, Oak Ridge, TN, for the U. S. Atomic Energy Commission, September 1968.

Engine Ingestion

43. Treager, I. E., *Aircraft Gas Turbine Engine Technology,* McGraw-Hill Book Company, New York, 1970.

44. Thompson, W. S., *Vulnerability Study of the J57 Non-Afterburner Turbojet Engine (U),* Ballistic Research Laboratory Memorandum Report No. 1867, August 1967.

45. Thompson, Walter S. and Wheeler, Raymond E., *Vulnerability Analysis of the J79 Augmented Turbojet Engine (U),* Ballistic Research Laboratories Memorandum Report No. 2082, December 1970.

46. McCormick, Jr., *Aerodynamics of V/STOL Flight,* Academic Press, New York, 1967.

47. Seddon J. and Goldsmith, E. L., *Intake Aerodynamics*, AIAA Education Series, New York, 1985.

Debris Generation

48. Sorge, M. E. and Johnson, C. G., *Space Debris Hazard Software: Program Impact Version 2.0 User's Guide*, Aerospace Report No. TOR-92(2909)-1, November 1991.

49. McKnight, Darren, Maher, Robert, and Nagl, Larry, *Refined Algorithms for Structural Breakup Due to Hypervelocity Impact,* Hypervelocity Impact Society Symposium, Santa Fe, NM, October 16-20, 1994, paper 082.

Overview

50. Cole, J. K. and Wolfe, W. P., *Hazards to People and Aircraft from Flight Test Debris Generated at High Altitudes,* Sandia National Laboratories Report SAND94-1723, August 1994.

Distribution:

Commander, White Sands Missile Range
STEWS-NRO-CF
Attn: Weston Wolff
WSMR, NM 88002-5113

Commander, White Sands Missile Range
STEWS-NRO-CF
Attn: Mike Meehan
WSMR, NM 88002-5113

Commander, White Sands Missile Range
STEWS-NRO-CF
Attn: Dave Donahe
WSMR, NM 88002-5113

45 SW/SEOO
Attn: Mike Campbell
1201 Minuteman Street
Patrick AFB, FL 32925-3239

45 SW/SEOO
Attn: Juri Kaevats
1201 Minuteman Street
Patrick AFB, FL 32925-3239

30 SW/SEY
Bldg. 7015, Section 3C
806 13th St. Suite 3
Attn: Martin Kinna
Vandenberg AFB, CA 93439-5230

Commander, USAKA
Attn: Steve LaPoint
P. O. Box 1003
APO AP 96555

USASSDC
CSSD-KH-SS
Attn: Jerry Esquibel
P. O. Box 1500
Huntsville, AL 35807

USASSDC
CSSD-TC-WS
Attn: Tom DeLong
P. O. Box 1500
Huntsville, AL 35807

NAWCWPN
Code 521300E
Attn: John Rogers
Point Mugu, CA 93042-5000

AFDTC/SEU
Attn: Ron Knight
505 N. Barrancas Ave., Suite 303
Eglin AFB, FL 32542-6817

NASA/Goddard Space Flight Center
Wallops Flight Facility (Code 821)
Attn: Dean Balach
Wallops Island, VA 23337

412 TW/TSRO
Attn: Steve Cronk
306 E. Popson Avenue
Edwards AFB, CA 93524-6680

ACTA, Inc.
23430 Hawthorne Blvd.
Skypark Bldg. 3, Suite 300
Attn: Jon Collins
Torrance, CA 90505

ACTA, Inc.
23430 Hawthorne Blvd.
Skypark Bldg. 3, Suite 300
Attn: Jerry Haber
Torrance, CA 90505

BMDO/AQT
7100 Defense Pentagon
The Pentagon, Room 1E-180
Attn: Tom Glenn
Washington, DC 20301-7100

Distribution: (Con't)

SRS Technologies
Attn: Jon Forst
1401 Wilson Blvd., Suite 1200
Arllington, VA 22209

Department of Transportation
FAA/AST-200
400 7th Street SW, Room 5402A
Attn: Carole Flores
Washington, DC 20590

APT Research, Inc.
Attn: Tom Pfitzer
555 Sparkman Drive, Suite 440
Huntsville, AL 35816-3421

APT Research, Inc.
Attn: Alice Correa
555 Sparkman Drive, Suite 440
Huntsville, AL 35816-3421

APT Research, Inc.
Attn: Dr. Paul Jaramillo
222 Bartlett #507
El Paso, TX 79912

TYBRIN Corporation
Attn: Brad Hill
4900 University Square
Suite 28
Huntsville, AL 35806

NAWC
Pacific Ranges and Facilities Dept.
Code 521310D
Attn: Everett Long
China Lake, CA 93555-6001

NAWCAD
Code 511200A, Mail Stop 3
Bldg. 1406
Attn: Mike Patterson
Patuxent River, MD 20670-5304

U.S. Army Test and Evaluation Command
AMSTE-TM-A
Attn: Doug Warrington
Aberdeen Proving Ground, MD 21005-5055

Internal Distribution:

MS 9005	2200	J. B. Wright
MS 0301	2400	D. J. Rigali
MS 0303	2411	J. L. McDowell
MS 0313	2412	D. L. Keese
MS 0308	2413	G. J. Hochrein
MS 0312	2414	W. E. Williamson
MS 0307	2417	E. W. Reece
MS 0309	2418	A. K. Miller
MS 0315	2419	R. G. Hay
MS 0314	2425	E. J. Schindwolf
MS 0842	2500	C. M. Hart
MS 0841	9100	P. J. Hommert
MS 0828	9102	R. D. Skocypec
MS 0441	9103	J. H. Biffle
MS 0828	9104	E. D. Gorham
MS 0826	9111	S. N. Kempka, Actg.
MS 0834	9112	A. C. Ratzel
MS 0835	9113	T. Bickel
MS 0827	9114	A. S. Geller, Actg.
MS 0825	9115	W. H. Rutledge
MS 0825	9115	J. K. Cole (10)
MS 0825	9115	T. M. Jordan-Culler (2)
MS 0825	9115	L. W. Young (2)
MS 0836	9116	C. W. Peterson
MS 0443	9117	H. S. Morgan
MS 0437	9118	R. K. Thomas
MS 0631	12300	W. C. Nickell
MS 0461	14700	C. A. Yarnall
1 MS 9018		Central Technical Files, 8940-2
5 MS 0899		Technical Library, 4414
2 MS 0619		Review & Approval Desk, 12690 For DOE/OSTI